PHOTONICS Research

Bound states of solitons in a harmonic graphene-mode-locked fiber laser

Bo Fu,[1,2] Jin Li,[3,4] Zhang Cao,[1,2] and Daniel Popa[3,*]

[1]Beijing Advanced Innovation Center for Big Data-Based Precision Medicine, Interdisciplinary Innovation Institute of Medicine and Engineering, Beihang University, Beijing 100191, China
[2]School of Instrumentation and Optoelectronic Engineering, Beihang University, Beijing 100191, China
[3]Department of Engineering, University of Cambridge, Cambridge CB3 0FA, UK
[4]e-mail: jl918@cam.ac.uk
*Corresponding author: dp387@cam.ac.uk

Received 26 October 2018; revised 23 November 2018; accepted 25 November 2018; posted 30 November 2018 (Doc. ID 348920); published 8 January 2019

We report bound states of solitons from a harmonic mode-locked fiber laser based on a solution-processed graphene saturable absorber. Stable soliton pairs, 26.2 ps apart, are generated with 720 fs duration. By simply increasing the pump power, the laser can also generate harmonic mode-locking with harmonics up to the 26th order (409.6 MHz repetition rate). This is a simple, low-cost, all-fiber, versatile multifunction ultrafast laser that could be used for many applications.

https://doi.org/10.1364/PRJ.7.000116

1. INTRODUCTION

Passively mode-locked fiber lasers are being extensively investigated due to their stable, alignment-free operation and compact design, making them attractive platforms for studying new pulse dynamics [1]. A common technique to generate ultrafast pulses in fiber lasers is soliton mode-locking, where an intracavity pulse is shaped by a balance of cavity dispersion and pulse-triggered nonlinear effects [1,2]. In this regime, a single pulse is normally circulating in the laser cavity, with a repetition rate (typically ~10 MHz) proportional to the inverse of the cavity length [1,2]. Higher repetition rates, desirable for applications such as two-photon microscopy [3], frequency comb [4], or fiber-optic communications [5], are possible by shortening the cavity length [2]. However, using this approach becomes challenging to compensate for dispersive effects [6]. A different technique relies on harmonic mode-locking (HML), where multiple pulses can circulate in the laser cavity with a pulse-to-pulse equal temporal spacing [7]. HML is typically achieved by increasing the intracavity power, which can contribute unbalanced nonlinear effects, finally causing the circulating pulse to break up into multiple pulses [8]. Depending on the physical effects governing the interaction between the as-formed pulses, these can self-organize into two or more closely (temporally) spaced pulses [9,10]. For example, cross-phase modulation between pulses can lead to the formation of a soliton pair, termed bound states (BS) or soliton molecules, with a temporal spacing ($\Delta\tau$) limited to several times of their pulse duration [11]. BS can then undergo many resonator round trips with constant $\Delta\tau$ and phase, i.e., they remain mutually coherent [12], with the resulting optical spectrum being modulated with a period $\Delta\nu = 1/\Delta\tau$ [13]. BS in passively mode-locked fiber lasers have been extensively studied in connection with their potential applications in optical communications and high-resolution spectroscopy [3,5]. Techniques as varied as nonlinear polarization rotation (NPR) [14,15], nonlinear optical loop mirrors (NOLMs) [16], semiconductor saturable absorber mirrors (SESAMs) [17], carbon nanomaterials [18,19], or other nanomaterials [20–22] have been used to study BS.

Among the techniques typically implemented to mode-lock fiber lasers [1], carbon nanotubes (CNTs) and graphene [23] have emerged as promising saturable absorbers (SAs), with a number of favorable properties for laser development [24–29]. In CNTs, broadband operation can be achieved by using a distribution of tube diameters [30], while this is an intrinsic property of graphene [31]. This, along with ultrafast recovery time [32], low saturation fluence [33], and ease of fabrication and integration into all-fiber configurations [23,34], makes graphene an excellent broadband SA. Consequently, mode-locked lasers using graphene SAs (GSAs) have been demonstrated for a broad spectral range [35–38]. A variety of techniques have been implemented in order to integrate graphene into lasers [23]. For example, graphene can be integrated into various optical components, with the possibility of controlling the modulation depth [39]. Because of their simplicity, low cost, and highly reliable performance, fabrication techniques based on graphene solutions [40] are widely used [41–45]. Although BS generation has been reported based on a multilayer GSA prepared by chemical vapor deposition (CVD) [19,46], HML was not

detected, which is required in order to generate high repetition rate pulses, important, e.g., for high-resolution spectroscopy [3,47]. Moreover, flakes grown by CVD require high substrate temperatures, followed by transfer to the target substrate [40]. Graphene-based solutions have the advantage of scalability, room temperature processing, and high yield, and do not require any substrate, which can be easily integrated into various systems [40].

Here, we use a graphene solution deposited on a fiber-based connector as SA. Based on this, we demonstrate BS HML of an all-fiber laser, achieving stable pulses with 720 fs and 409.6 MHz repetition rate. Such a simple and environmentally robust light source could be used for a variety of applications, including nonlinear imaging and spectroscopy.

2. EXPERIMENTAL SETUP

The GSA is prepared by using a reduced graphene oxide solution based on a modified Hummers method [48]. Graphite oxide is prepared from natural graphite powder stirred into a mixture of sulfuric acid (98 wt.%) and hydrogen peroxide (30 wt.%) (20:1 by volume), followed by rinsing with deionized water, and heating (after evaporation) at 1000°C for 30 s. Graphite oxide is then exfoliated via ultrasonic treatment in a solution of deionized water, and subsequently reduced by hydrazine hydrate at 95°C for 12 h. Finally, a graphene ethanol solution is obtained by ultrasonication for 3 h. Absorption measurements, presented in Fig. 1(a), show a featureless spectrum from 250 to 1600 nm (the alcohol contribution was subtracted), with the UV peak a signature of the van Hove singularity in the graphene density of states [49].

To integrate the graphene solution in our fiber laser, we use a simple method based on optical deposition [50,51]. A fiber connector for physical contact (FC/PC), to be used in the laser, is immersed in the graphene solution. Tens of mW of optical power is then launched into the FC/PC from a 1550 nm continuous wave (CW) laser for ~10 min. After alcohol evaporation, a graphene film is obtained at the center of the fiber core

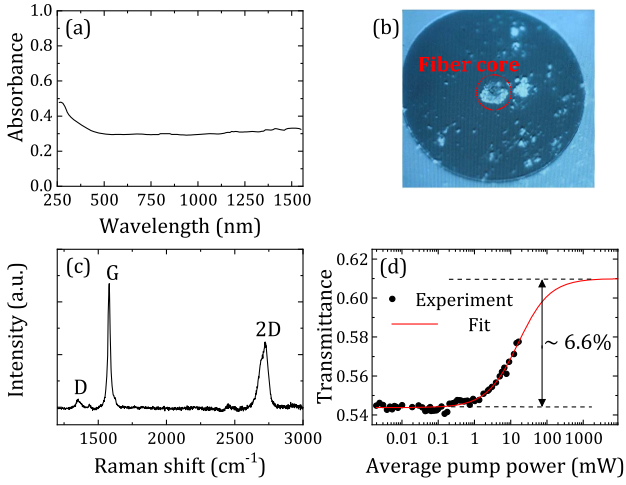

Fig. 1. (a) Linear absorption of the graphene solution (alcohol contribution subtracted); (b) GSA film optically deposited on fiber tip; (c) Raman spectrum of GSA film on fiber tip; (d) nonlinear transmittance at the laser operating wavelength.

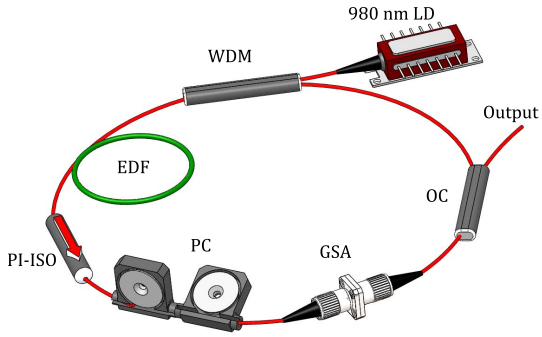

Fig. 2. All-fiber laser schematic. LD, laser diode; WDM, wavelength-division multiplexer; EDF, Er-doped fiber; PI-ISO, polarization-insensitive isolator; PC, polarization controller; GSA, graphene saturable absorber; OC, optical coupler.

on the FC/PC tip, as shown in Fig. 1(b). To check the film quality after deposition, we characterize it by Raman spectroscopy at 514 nm. Figure 1(c) plots the Raman spectrum of the graphene film on the FC/PC tip. A small D peak (~1354 cm^{-1}) indicates negligible graphene defects [52]. Next, we measure the GSA nonlinear optical transmittance with a pulsed fiber laser (Calmar), which delivers 220 fs pulses with 24.97 MHz repetition rate at 1550 nm. The optical transmittance is determined by monitoring the input and output power, and is shown in Fig. 1(d). An ~3.2% change in transmittance is noticed for an input average power of 16.5 mW. Further increasing the transmittance is feasible, but limited in our setup by the maximum available peak power. The GSA modulation depth is estimated at ~6.6% [53], which is preferred for mode locking of fiber lasers [54], which typically operate with higher gain and cavity losses [1] than their solid-state counterparts [55]. The GSA has ~2.7 dB insertion loss.

The experimental configuration of our all-fiber laser is shown in Fig. 2. We use a 48-cm-long erbium-doped fiber (EDF, Er110-4/125, with 110 dB/m absorption at 1530 nm, and 12 ps^2/km second-order dispersion) as a gain medium pumped by a 980 nm CW laser diode (LD) through a fused wavelength-division multiplexer (WDM). The rest of the cavity is formed by ~12.7 m of standard single-mode fiber (SMF-28 with ~ – 23 ps^2/km second-order dispersion). This gives –0.29 ps^2 net intracavity second-order dispersion, typical of soliton lasers [1]. Unidirectional operation is ensured by a polarization-insensitive isolator (PI-ISO), while a polarization controller (PC) is used for mode-locking optimization and stabilization. The 10% port of a fused coupler provides the laser output. The laser operation is monitored by an optical spectrum analyzer, a 2 GHz oscilloscope via a 1 GHz photodetector, a second-harmonic-generation (SHG) autocorrelator, and a radio frequency (RF) signal analyzer.

3. RESULTS AND DISCUSSION

Mode-locking self-starts at ~50 mW pump power (P_p). A set of typical results is shown in Fig. 3. The output optical spectrum, shown in Fig. 3(a), has a 3.1 nm full width at half-maximum (FWHM) centered at $\lambda = 1558$ nm. The spectrum features Kelly sidebands, a signature of soliton-like

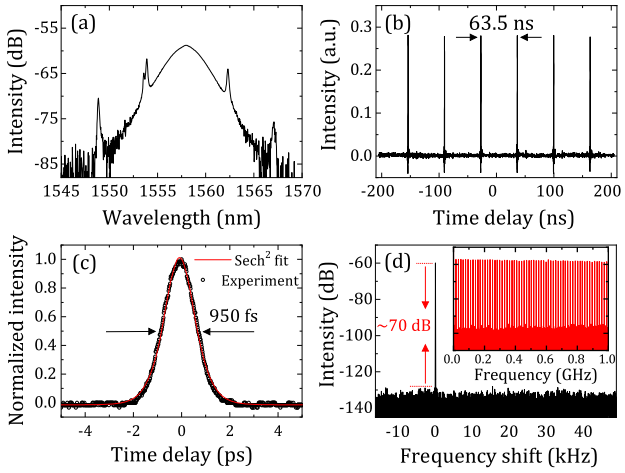

Fig. 3. Fundamental mode-locking experimental results. (a) Optical spectrum; (b) temporal waveform; (c) pulse profile; (d) RF spectrum with 10 Hz resolution (inset, 1000 MHz span).

operation [56]. The fundamental repetition rate, shown in Fig. 3(b), is 15.75 MHz, as determined by the 13.2 m cavity length. Figure 3(c) shows the intensity autocorrelation trace with 950 fs pulse duration, calculated by fitting a sech^2 profile to the pulse, as expected for soliton-like mode-locking [6]. The time-bandwidth product (TBP) is 0.354, close to the theoretical value (0.315) for transform-limited sech^2-shaped pulses. The output pulse energy is 11.2 pJ. The laser stability is characterized by RF measurements [57]. Figure 3(d) plots the RF spectrum around the fundamental repetition rate recorded with 10 Hz resolution. A ~70 dB signal-to-noise ratio (SNR) indicates low-amplitude fluctuations [57]. There is no spectral modulation over 1 GHz [see inset of Fig. 3(d)], which, when combined with long-range autocorrelation measurements, rules out multiple pulsing [57].

We investigate BS operation. By slightly increasing P_p and tuning the PC, we observe spectral periodic modulations, a typical signature of BS interference [9,11]. We find the spectral modulations, shown in Figs. 4(a)–4(c), dependent on the intracavity polarization state, as expected for BS operation [18]. Further tuning the PC, the CW peaks (an indication of laser stability [58]) shown in Figs. 4(a) and 4(b), are eliminated. A resulting spectrum is shown in Fig. 4(c), when the laser delivers two pulse molecules, i.e., BS [11]. A set of typical BS results is shown in Figs. 4(c)–4(f). The spectrum in Fig. 4(c) reveals a modulation period $\Delta\nu = \Delta\lambda\frac{\nu}{\lambda} = 38.19\,\mathrm{GHz}$, for $\Delta\lambda = 0.31$ nm at $\lambda = 1560$ nm. The corresponding intensity autocorrelation trace is shown in Fig. 4(d), with $\Delta\tau = 26.2$ ps time delay between pulses (center to side peaks), in agreement with the spectral modulation period (i.e., $\Delta\nu = 1/\Delta\tau$). The pulse duration, shown in the inset of Fig. 4(d), is 720 fs. The pulses circulate in the cavity at 15.75 MHz repetition rate (63.5 ns delay), according to its length ~13.2 m, as shown in Fig. 4(e). An SNR of ~68 dB, shown in Fig. 4(f), recorded with 10 Hz resolution, confirms BS operation stability [57].

We investigate HML operation by further increasing P_p and tuning the PC. HML harmonics can be generated with orders from the first to the 26th. Figure 5(a) shows the

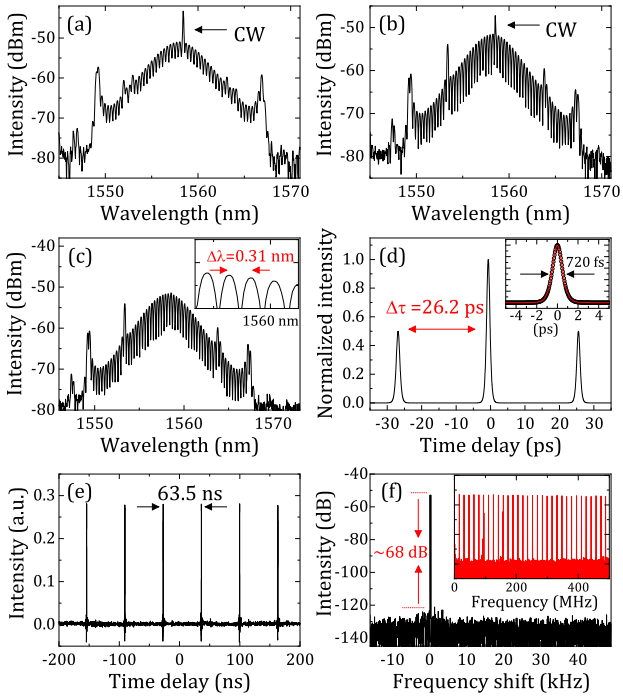

Fig. 4. BS experimental results. (a), (b), and (c) BS spectral modulations as functions of intracavity polarization, with a stable CW-free spectrum shown in (c) (inset, spectral magnification around the central wavelength, 1558 nm); (d) autocorrelation trace of the pulses (inset, pulse profile). The pulse separation $\Delta\tau$ modulates the spectrum with a period of $1/\Delta\tau$. (e) Temporal waveform of the intracavity circulating pulses; (f) RF spectrum with 10 Hz resolution (inset, 500 MHz span).

HML spectrum centered at 1558 nm with 3.4 nm FWHM for P_p ~310 mW (inset, the intensity autocorrelation trace for the 26th harmonic pulses). The pulse duration is 840 fs, corresponding to a TBP of 0.343, in agreement with that of fundamental mode-locking. The repetition rate is 409.6 MHz,

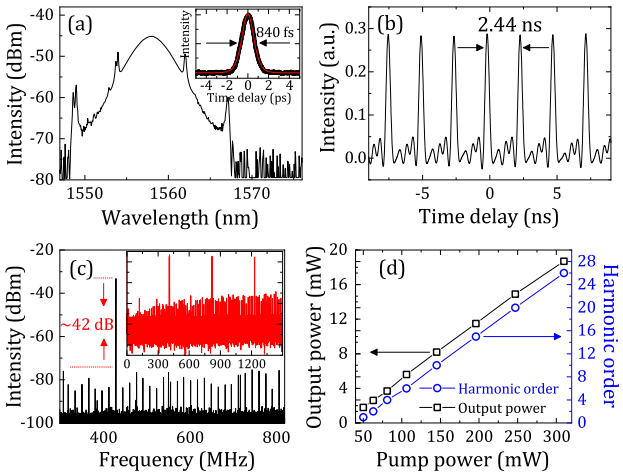

Fig. 5. HML experimental results. (a) Optical spectrum (inset, pulse profile); (b) temporal waveform; (c) RF spectrum with 20 kHz resolution (inset, 1500 MHz span); (d) output power and harmonic order as functions of pump power.

corresponding to ~2.44 ns delay between pulses [Fig. 5(b)], i.e., the 26th harmonic. Figure 5(c) shows an ~42 dB supermode suppression, for the 26th harmonic [recorded over 800 MHz span with 20 kHz resolution bandwidth (inset, 1.5 GHz span)] and an ~65 dB background noise, indicating stable HML operation of our laser [59]. We also investigate the harmonic order and the output power as functions of P_p, as shown in Fig. 5(d). Depending on the PC orientation, the laser can operate either in normal or BS mode-locking when P_p is ~50 to 63 mW. Further increasing P_p results in HML operation, with the second harmonic achieved for P_p ~63 mW. As indicated in Fig. 5(d), the harmonic order and output power increase gradually with P_p up to the 26th harmonic, when P_p is ~310 mW, giving ~18.7 mW output power. Higher P_p, limited in our case to ~320 mW, could further increase the harmonic order. We monitor the laser operation for a 4-h period and observe power variations below ~0.2% for different mode-locking states. We did not observe any damage to the GSA.

Compared to NPR, NOLMs, or SESAMs, our all-fiber design, exploiting a GSA, is simpler to assemble, needing no critical alignment. BS graphene-based all-fiber setups have been reported [19,46]; however, the use of multilayer CVD graphene structures complicates the fabrication process. Compared to CNT-based SAs, which limit the operation wavelength, our GSA can operate at any wavelength.

4. CONCLUSIONS

We report the generation of BS of solitons and HML from a graphene mode-locked all-fiber laser. BS of solitons are observed by adjusting the laser intracavity polarization. HML, with orders from the first to the 26th, is also detected by further increasing the pump power, making the laser attractive for applications such as nonlinear imaging or spectroscopy.

Funding. National Natural Science Foundation of China (NSFC) (61575106); Beihang University (BUAA); Beijing Advanced Innovation Center for Big Data-Based Precision Medicine (Ultrafast Pulsed Fiber Lasers and Applications); School of Instrumentation and Optoelectronic Engineering.

REFERENCES

1. M. E. Fermann and I. Hartl, "Ultrafast fibre lasers," Nat. Photonics **7**, 868–874 (2013).
2. I. N. Duling, "Subpicosecond all-fibre erbium laser," Electron. Lett. **27**, 544–545 (1991).
3. J. Bewersdorf and S. W. Hell, "Picosecond pulsed two-photon imaging with repetition rates of 200 and 400 MHz," J. Microsc. **191**, 28–38 (1998).
4. S. A. Diddams, L. Hollberg, and V. Mbele, "Molecular fingerprinting with the resolved modes of a femtosecond laser frequency comb," Nature **445**, 627–630 (2007).
5. H. A. Haus and W. S. Wong, "Solitons in optical communications," Rev. Mod. Phys. **68**, 423–444 (1996).
6. G. P. Agrawal, *Applications of Nonlinear Fiber Optics*, 2nd ed. (Elsevier Academic, 2008), pp. 1–508.
7. A. B. Grudinin, D. J. Richardson, and D. N. Payne, "Passive harmonic modelocking of a fibre soliton ring laser," Electron. Lett. **29**, 1860–1861 (1993).
8. L. Nelson, D. Jones, K. Tamura, H. Haus, and E. Ippen, "Ultrashort-pulse fiber ring lasers," Appl. Phys. B **65**, 277–294 (1997).
9. B. A. Malomed, "Bound solitons in the nonlinear Schrödinger-Ginzburg-Landau equation," Phys. Rev. A **44**, 6954–6957 (1991).
10. A. Komarov, K. Komarov, and F. Sanchez, "Harmonic passive mode locking of bound-soliton structures in fiber lasers," Opt. Commun. **354**, 158–162 (2015).
11. D. Y. Tang, W. S. Man, H. Y. Tam, and P. D. Drummond, "Observation of bound states of solitons in a passively mode-locked fiber laser," Phys. Rev. A **64**, 033814 (2001).
12. P. Grelu, F. Belhache, F. Gutty, and J. M. Soto-Crespo, "Phase-locked soliton pairs in a stretched-pulse fiber laser," Opt. Lett. **27**, 966–968 (2002).
13. G. Herink, F. Kurtz, B. Jalali, D. R. Solli, and C. Ropers, "Real-time spectral interferometry probes the internal dynamics of femtosecond soliton molecules," Science **356**, 50–54 (2017).
14. H. Qin, X. Xiao, P. Wang, and C. Yang, "Observation of soliton molecules in a spatiotemporal mode-locked multimode fiber laser," Opt. Lett. **43**, 1982–1985 (2018).
15. P. Wang, C. Bao, B. Fu, X. Xiao, P. Grelu, and C. Yang, "Generation of wavelength-tunable soliton molecules in a 2-μm ultrafast all-fiber laser based on nonlinear polarization evolution," Opt. Lett. **41**, 2254–2257 (2016).
16. N. H. Seong and D. Y. Kim, "Experimental observation of stable bound solitons in a figure-eight fiber laser," Opt. Lett. **27**, 1321–1323 (2002).
17. B. Ortaç, A. Zaviyalov, C. K. Nielsen, O. Egorov, R. Iliew, J. Limpert, F. Lederer, and A. Tünnermann, "Observation of soliton molecules with independently evolving phase in a mode-locked fiber laser," Opt. Lett. **35**, 1578–1580 (2010).
18. X. Liu, X. Yao, and Y. Cui, "Real-time observation of the buildup of soliton molecules," Phys. Rev. Lett. **121**, 023905 (2018).
19. L. Gui, X. Li, X. Xiao, H. Zhu, and C. Yang, "Widely spaced bound states in a soliton fiber laser with graphene saturable absorber," IEEE Photon. Technol. Lett. **25**, 1184–1187 (2013).
20. P. Wang, K. Zhao, L. Gui, X. Xiao, and C. Yang, "Self-organized structures of soliton molecules in 2-μm fiber laser based on MoS_2 saturable absorber," IEEE Photon. Technol. Lett. **30**, 1210–1213 (2018).
21. X. Li, K. Xia, D. Wu, Q. Nie, and S. Dai, "Bound states of solitons in a fiber laser with a microfiber-based WS_2 saturable absorber," IEEE Photon. Technol. Lett. **29**, 2071–2074 (2017).
22. Y. Wang, D. Mao, X. Gan, L. Han, C. Ma, T. Xi, Y. Zhang, W. Shang, S. Hua, and J. Zhao, "Harmonic mode locking of bound-state solitons fiber laser based on MoS_2 saturable absorber," Opt. Express **23**, 205–210 (2015).
23. A. Martinez and Z. Sun, "Nanotube and graphene saturable absorbers for fibre lasers," Nat. Photonics **7**, 842–845 (2013).
24. Z. Zhang, D. Popa, V. J. Wittwer, S. Milana, T. Hasan, Z. Jiang, A. C. Ferrari, and F. O. Ilday, "All-fiber nonlinearity- and dispersion-managed dissipative soliton nanotube mode-locked laser," Appl. Phys. Lett. **107**, 241107 (2015).
25. R. I. Woodward, E. J. R. Kelleher, D. Popa, T. Hasan, F. Bonaccorso, A. C. Ferrari, S. V. Popov, and J. R. Taylor, "Scalar nanosecond pulse generation in a nanotube mode-locked environmentally stable fiber laser," IEEE Photon. Technol. Lett. **26**, 1672–1675 (2014).
26. R. Mary, G. Brown, S. J. Beecher, R. R. Thomson, D. Popa, Z. Sun, F. Torrisi, T. Hasan, S. Milana, F. Bonaccorso, A. C. Ferrari, and A. K. Kar, "Evanescent-wave coupled right angled buried waveguide: applications in carbon nanotube mode-locking," Appl. Phys. Lett. **103**, 221117 (2013).
27. K. Kieu and F. W. Wise, "All-fiber normal-dispersion femtosecond laser," Opt. Express **16**, 11453–11458 (2008).
28. C. S. Jun, S. Y. Choi, F. Rotermund, B. Y. Kim, and D.-I. Yeom, "Toward higher-order passive harmonic mode-locking of a soliton fiber laser," Opt. Lett. **37**, 1862–1864 (2012).
29. L. Gui, X. Xiao, and C. Yang, "Observation of various bound solitons in a carbon-nanotube-based erbium fiber laser," J. Opt. Soc. Am. B **30**, 158–164 (2013).
30. R. Going, D. Popa, F. Torrisi, Z. Sun, T. Hasan, F. Wang, and A. C. Ferrari, "500 fs wideband tunable fiber laser mode-locked by nanotubes," Phys. E **44**, 1078–1081 (2012).

31. Z. Sun, T. Hasan, F. Torrisi, D. Popa, G. Privitera, F. Wang, F. Bonaccorso, D. M. Basko, and A. C. Ferrari, "Graphene mode-locked ultrafast laser," ACS Nano **4**, 803–810 (2010).
32. D. G. Purdie, D. Popa, V. J. Wittwer, Z. Jiang, G. Bonacchini, F. Torrisi, S. Milana, E. Lidorikis, and A. C. Ferrari, "Few-cycle pulses from a graphene mode-locked all-fiber laser," Appl. Phys. Lett. **106**, 253101 (2015).
33. D. Popa, Z. Sun, F. Torrisi, T. Hasan, F. Wang, and A. C. Ferrari, "Sub 200 fs pulse generation from a graphene mode-locked fiber laser," Appl. Phys. Lett. **97**, 203106 (2010).
34. G. Sobon, J. Sotor, and K. M. Abramski, "Passive harmonic mode-locking in Er-doped fiber laser based on graphene saturable absorber with repetition rates scalable to 2.22 GHz," Appl. Phys. Lett. **100**, 161109 (2012).
35. B. Fu, Y. Hua, X. Xiao, H. Zhu, Z. Sun, and C. Yang, "Broadband graphene saturable absorber for pulsed fiber lasers at 1, 1.5, and 2-μm," IEEE J. Sel. Top. Quantum Electron. **20**, 411–415 (2014).
36. I. H. Baek, H. W. Lee, S. Bae, B. H. Hong, Y. H. Ahn, D.-I. Yeom, and F. Rotermund, "Efficient mode-locking of sub-70-fs Ti:sapphire laser by graphene saturable absorber," Appl. Phys. Express **5**, 032701 (2012).
37. M. N. Cizmeciyan, J. W. Kim, S. Bae, B. H. Hong, F. Rotermund, and A. Sennaroglu, "Graphene mode-locked femtosecond Cr:ZnSe laser at 2500 nm," Opt. Lett. **38**, 341–343 (2013).
38. G. Zhu, X. Zhu, F. Wang, S. Xu, Y. Li, X. Guo, K. Balakrishnan, R. A. Norwood, and N. Peyghambarian, "Graphene mode-locked fiber laser at 2.8 μm," IEEE Photon. Technol. Lett. **28**, 7–10 (2016).
39. C. A. Zaugg, Z. Sun, V. J. Wittwer, D. Popa, S. Milana, T. S. Kulmala, R. S. Sundaram, M. Mangold, O. D. Sieber, M. Golling, Y. Lee, J. H. Ahn, A. C. Ferrari, and U. Keller, "Ultrafast and widely tuneable vertical-external-cavity surface-emitting laser, mode-locked by a graphene-integrated distributed Bragg reflector," Opt. Express **21**, 31548–31559 (2013).
40. F. Bonaccorso, A. Lombardo, T. Hasan, Z. Sun, L. Colombo, and A. C. Ferrari, "Production and processing of graphene and 2d crystals," Mater. Today **15**, 564–589 (2012).
41. Z. Luo, M. Zhou, J. Weng, G. Huang, H. Xu, C. Ye, and Z. Cai, "Graphene-based passively *Q*-switched dual-wavelength erbium-doped fiber laser," Opt. Lett. **35**, 3709–3711 (2010).
42. A. Martinez, K. Fuse, B. Xu, and S. Yamashita, "Optical deposition of graphene and carbon nanotubes in a fiber ferrule for passive mode-locked lasing," Opt. Express **18**, 23054–23061 (2010).
43. D. Popa, Z. Jiang, G. E. Bonacchini, Z. Zhao, L. Lombardi, F. Torrisi, A. K. Ott, E. Lidorikis, and A. C. Ferrari, "A stable, power scaling, graphene-mode-locked all-fiber oscillator," Appl. Phys. Lett. **110**, 243102 (2017).
44. F. Torrisi, D. Popa, S. Milana, Z. Jiang, T. Hasan, E. Lidorikis, and A. C. Ferrari, "Stable, surfactant-free graphene-styrene methylmethacrylate composite for ultrafast lasers," Adv. Opt. Mater. **4**, 1088–1097 (2016).
45. D. Popa, D. Viola, G. Soavi, B. Fu, L. Lombardi, S. Hodge, D. Polli, T. Scopigno, G. Cerullo, and A. C. Ferrari, "Coherent Raman spectroscopy with a graphene-synchronized all-fiber laser," in *Conference on Lasers and Electro-Optics* (Optical Society of America, 2017), paper JTu5A.2.
46. L. Gui and C. Yang, "Soliton molecules with ±π/2, 0, and π phase differences in a graphene-based mode-locked erbium-doped fiber laser," IEEE Photon. J. **10**, 1502609 (2018).
47. T. Wu, K. Chen, H. Zhao, W. Zhang, Y. Li, and H. Wei, "Flexible dual-soliton manipulation for coherent anti-Stokes Raman scattering spectroscopy," Opt. Express **26**, 22001–22010 (2018).
48. W. S. Hummers and R. E. Offeman, "Preparation of graphitic oxide," J. Am. Chem. Soc. **80**, 1339 (1958).
49. V. G. Kravets, A. N. Grigorenko, R. R. Nair, P. Blake, S. Anissimova, K. S. Novoselov, and A. K. Geim, "Spectroscopic ellipsometry of graphene and an exciton-shifted van Hove peak in absorption," Phys. Rev. B **81**, 155413 (2010).
50. K. Kashiwagi, S. Yamashita, and S. Y. Set, "*In-situ* monitoring of optical deposition of carbon nanotubes onto fiber end," Opt. Express **17**, 5711–5715 (2009).
51. J. W. Nicholson, R. S. Windeler, and D. J. DiGiovanni, "Optically driven deposition of single-walled carbon-nanotube saturable absorbers on optical fiber end-faces," Opt. Express **15**, 9176–9183 (2007).
52. A. C. Ferrari, J. C. Meyer, V. Scardaci, C. Casiraghi, M. Lazzeri, F. Mauri, S. Piscanec, D. Jiang, K. S. Novoselov, S. Roth, and A. K. Geim, "Raman spectrum of graphene and graphene layers," Phys. Rev. Lett. **97**, 187401 (2006).
53. H. A. Haus, "Theory of mode locking with a fast saturable absorber," J. Appl. Phys. **46**, 3049–3058 (1975).
54. A. Cabasse, G. Martel, and J. Oudar, "High power dissipative soliton in an erbium-doped fiber laser mode-locked with a high modulation depth saturable absorber mirror," Opt. Express **17**, 9537–9542 (2009).
55. W. Koechner, *Solid-State Laser Engineering*, 6th ed., Springer Series in Optical Sciences (Springer, 2006).
56. S. M. J. Kelly, "Characteristic sideband instability of periodically amplified average soliton," Electron. Lett. **28**, 806–807 (1992).
57. D. von der Linde, "Characterization of the noise in continuously operating mode-locked lasers," Appl. Phys. B **39**, 201–217 (1986).
58. R. Iegorov, T. Teamir, G. Makey, and F. O. Ilday, "Direct control of mode-locking states of a fiber laser," Optica **3**, 1312–1315 (2016).
59. A. B. Grudinin and S. Gray, "Passive harmonic mode locking in soliton fiber lasers," J. Opt. Soc. Am. B **14**, 144–154 (1997).